Published in final edited form as:
FEBS J. 2005 October ; 272(20): 5265–5277.

Molecular basis for substrate recognition and drug resistance from 1.1 to 1.6 Å resolution crystal structures of HIV-1 protease mutants with substrate analogs

Yunfeng Tie[1], **Peter I. Boross**[2,3], **Yuan-Fang Wang**[2], **Laquasha Gaddis**[2], **Fengling Liu**[2], **Xianfeng Chen**[2], **Jozsef Tozser**[3], **Robert W. Harrison**[2,4], and **Irene T. Weber**[1,2]

1*Department of Chemistry, Molecular Basis of Disease, Georgia State University, Atlanta, GA, USA*

2*Department of Biology, Molecular Basis of Disease, Georgia State University, Atlanta, GA, USA*

3*Department of Biochemistry and Molecular Biology, Faculty of Medicine, University of Debrecen, Hungary*

4*Department of Computer Science, Molecular Basis of Disease, Georgia State University, Atlanta, GA, USA*

Abstract

HIV-1 protease (PR) and two drug-resistant variants – PR with the V82A mutation (PR_{V82A}) and PR with the I84V mutation (PR_{I84V}) – were studied using reduced peptide analogs of five natural cleavage sites (CA-p2, p2-NC, $p6^{pol}$-PR, p1-p6 and NC-p1) to understand the structural and kinetic changes. The common drug-resistant mutations V82A and I84V alter residues forming the substrate-binding site. Eight crystal structures were refined at resolutions of 1.10–1.60 Å. Differences in the PR–analog interactions depended on the peptide sequence and were consistent with the relative inhibition. Analog $p6^{pol}$-PR formed more hydrogen bonds of P2 Asn with PR and fewer van der Waals contacts at P1′ Pro compared with those formed by CA-p2 or p2-NC in PR complexes. The P3 Gly in p1-p6 provided fewer van der Waals contacts and hydrogen bonds at P2–P3 and more water-mediated interactions. PR_{I84V} showed reduced van der Waals interactions with inhibitor compared with PR, which was consistent with kinetic data. The structures suggest that the binding affinity for mutants is modulated by the conformational flexibility of the substrate analogs. The complexes of PR_{V82A} showed smaller shifts of the main chain atoms of Ala82 relative to PR, but more movement of the peptide analog, compared to complexes with clinical inhibitors. PR_{V82A} was able to compensate for the loss of interaction with inhibitor caused by mutation, in agreement with kinetic data, but substrate analogs have more flexibility than the drugs to accommodate the structural changes caused by mutation. Hence, these structures help to explain how HIV can develop drug resistance while retaining the ability of PR to hydrolyze natural substrates.

Keywords

catalysis; crystal structure; drug resistance; HIV-1 protease; substrate analog

Abbreviations

Nle, norleucine; PR, wild type HIV-1 protease; PR_{V82A}, PR with the V82A mutation; PR_{I84V}, PR with the I84V mutation

Correspondence I. T. Weber, Department of Biology, PO Box 4010, Georgia State University, Atlanta, GA 30302-4010, USA, Fax: +1 404 651 2509, Tel: +1 404 651 0098, E-mail:iweber@gsu.edu.

HIV-1 protease (PR) plays an essential role in the viral replication cycle because it cleaves the Gag and Gag– Pol polyproteins to yield the viral structural and functional proteins during maturation [1]. The catalytic activity of the mature PR and ordered processing of the polyproteins have been shown to be critical for the liberation of infective progeny virus [2]. Thus, inhibitors of HIV-1 PR are very effective antiviral drugs that prolong the life of patients with acquired immune-deficiency syndrome. However, the long-term use of these drugs is limited by the development of cross resistance and multidrug-resistant variants during treatment.

HIV-1 PR has 99 amino acid residues and is enzymatically active as a homodimer. Crystal structures have been determined for HIV PR in the presence and absence of inhibitor [3]. Mutations in the substrate-binding site can cause resistance by reducing the PR-binding affinity by two- to fivefold for inhibitors [4]. Resistant mutations are commonly observed at D30, M46, I50, V82 and I84 [5,6]. Mutations of residue 82 show decreased susceptibility to indinavir, ritonavir and lopinavir *in vitro*. The most common mutation at position V82A is observed predominantly in HIV-1 isolates from patients receiving treatment with indinavir and ritonavir. Mutation I84V has been reported in patients receiving indinavir, ritonavir, saquinavir and amprenavir. I84V tends to develop in isolates that already have the mutation L90M and is rarely the first major mutation to develop in patients receiving a PR inhibitor [7].

HIV PR hydrolyzes several different cleavage sites in the natural polyprotein substrates that show little sequence similarity. The mechanisms for how the resistant mutants maintain sufficient enzymatic activity for viral replication can be better understood by studying the structures of PR with natural cleavage sites. Two strategies have been applied to overcome the difficulty of crystallizing catalytically active enzyme with peptide substrates. Our strategy has been to analyze structures of active PR with substrate analogs, while other groups have used an alternative strategy of crystallizing an inactive enzyme with peptide substrates. Crystal structures at ≈1.9 Å resolution have been reported of the inactive PR variant (D25N) in complex with peptides representing eight cleavage sites, and inactive mutant V82A–D25N with patients [8–10]. We have reported crystal structures of PR, single mutants in complex with substrate analogs CA-p2 and p2-NC, and double mutants with CA-p2 at resolutions ranging from 2.2 to 1.2 Å [11–13]. Here, we present higher resolution crystal structures of PR and the common drug-resistant variants – PR with the V82A mutation (PR_{V82A}) and PR with the I84V mutation (PR_{I84V}) – in complexes with reduced peptide analogs that represent the CA-p2, p2-NC, $p6^{pol}$-PR and p1-p6 polyprotein cleavage sites. These structures and kinetic data provide details of the PR interaction with reaction intermediates and a better understanding of the substrate specificity. Comparison of protease complexes with clinical inhibitors will assist in the structure-based design of more potent antiviral inhibitors.

Results and Discussion

Inhibition of PR, PR_{V82A} and PR_{I84V}

The reduced peptide analogs represent five different HIV-1 cleavage sites (Table 1). The p2-NC site is the first and CA-p2 the last in sequential processing of the Gag precursor [14]. Cleavage of $p6^{pol}$-PR is essential for the release of mature active protease [15]. Mutations in the NC-p1 and p1-p6 sites contribute to drug resistance both *in vitro* and *in vivo* [16–18]. These two cleavage sites show significant sequence polymorphism [19,20], and the specificity of cleavage has been studied with PR and several mutants [21]. CA-p2 and p2-NC were the two shortest peptides, extending from P3 to P4′ and from P3 to P3′, respectively. The analogs NC-p1 and p1-p6 extended from P5 to P5′, while $p6^{pol}$-PR extended from P5 to P6′ because lysine was added to provide greater solubility.

The catalytic activities of PR and of the mutants PR_{V82A} and PR_{I84V} were found to be competitively inhibited by the five substrate analogs (Table 1). Previous studies have demonstrated that reduced peptide bond-containing analogs of natural cleavage site sequences act as competitive inhibitors of HIV-1 PR [22,23], and the same type of inhibition was assumed, in this study, for the mutants. The inhibition constants for PR were in the order CA-p2 < p2-NC < $p6^{pol}$- PR < p1-p6 < NC-p1. The CA-p2 analog was the best inhibitor of PR and the mutants. The NC-p1 analog had no substantial inhibition for all enzymes at a peptide concentration of 0.5 mM. PR_{V82A} was better inhibited than PR (approximately threefold) by all the analogs, except for $p6^{pol}$-PR. PR_{I84V} was poorly inhibited, relative to PR, for all analogs, with two to sixfold higher K_i values, and no significant inhibition by p1-p6. This variation in K_i was smaller than observed for the clinical inhibitors, which showed two- to 11-fold relative inhibition of the mutants PR_{V82A} or PR_{I84V} compared with wild-type PR [24].

Description of the high-resolution crystal structures

Eight crystal structures were determined of PR and of the drug-resistant mutants, PR_{V82A} and PR_{I84V}, in the complexes with four different substrate analogs. Crystallographic statistics are summarized in Table 2. Seven of these are new structures, while the PR–CA-p2 complex was determined at the higher resolution of 1.4 Å compared with 1.9 Å for the previously reported structure [12]. Crystals and diffraction data were obtained for PR complexed with the NC-p1 analog; however, the electron density was disordered and not interpretable for the analog, probably as a result of weak binding and consistent with the high K_i values of >500 μM. Diffraction quality crystals were not obtained for the other possible complexes. The asymmetric unit of the crystals contained a PR dimer with the residues in the two subunits numbered 1–99 and 1′– 99′. All structures are in space group $P2_12_12$ and were refined to R-factors of 0.12–0.18, including solvent molecules, and anisotropic B-factors. The resolution ranged from 1.10 to 1.60 Å. The complex PR_{V82A}–p2-NC was determined at 1.1 Å resolution, the highest resolution to date for a substrate–analog complex. The quality of the electron density map is shown in Fig. 1. The crystal structures showed clear electron density for all the PR atoms, P4-P4′ residues in the peptide analog, and solvent molecules. All the peptide analogs, except for p2-NC, showed two pseudosymmetric conformations bound to both subunits of the PR dimer. The $p6^{pol}$-PR and p1-p6 analogs had 11 and 10 residues, respectively, compared with six to seven for the CA-p2 and p2-NC analogs. The longer analogs extended out of the PR-binding pocket and showed poor electron density at both termini. The average B-factors ranged from 8.0 $Å^2$ at the higher resolutions to 22.4 $Å^2$ at the lower resolutions for protein main chain atoms, and 10.6–29.9 $Å^2$ for protein side chain and inhibitor atoms.

Alternate conformations were modeled for the side chain atoms of ≈30 residues in all the crystal structures, based on the shape of the electron density (Fig. 2). Only Lys7 had alternate conformations in both subunits of all structures, while Met46 had alternate conformations in all but one subunit. Most of these alternate conformations were observed for residues with longer and flexible side chains, such as Lys. The number of alternate conformations was in the order of Lys (68 with alternate conformations), Ile (41), Glu (35) and Met (15), followed by Gln, Arg, Ser and Leu at about 10 each. Some residues, including 33′, 34′ and 35′ were observed to have two conformations only in one subunit of the dimer. These residues were located on the PR surface and were either very flexible or interacted with symmetry related molecules. The presence of alternate conformations of side chains for Leu23, Lys45/45′, Met46/46′, Ile50/50′, Val82/82′ and Ile84/84′ in the inhibitor binding site was consistent with previous descriptions [12,25]. Alternate positions with a 180° flip of the main chain atoms of Ile50 and 50′ were observed in complexes PR–p1-p6, PR_{V82A}–p1-p6, PR–$p6^{pol}$-PR and PR_{V82A}–$p6^{pol}$-PR, as described previously [25].

Overall comparison of the crystal structures

Comparison of ligand bound and unliganded PR structures [26,27] and theoretical studies [28,29] have suggested that resistant mutations can alter the conformational flexibility of the PR flaps and dimer interface. Our high resolution, low temperature crystal structures of liganded PR showed mostly static disorder, which does not address the question of dynamic flexibility. Moreover, the PR and mutant dimers shared almost identical backbone structures, with the root mean square deviation for all Cα atoms ranging from 0.09 to 0.26 Å compared with the PR–p2-NC complex (Fig. 3). The least variation was observed for the complexes with p2-NC. The deviations for residues in subunit A (within 1 Å) were larger than those of subunit B (within 0.8 Å). Larger deviations for all the structures were located at external loop residues 38–41 and residues 79–84 near the mutations. The biggest difference from PR–p2-NC was observed for the complexes with the $p6^{pol}$-PR analog, and occurred at residues 47–53 in the hairpin loop that links two β-strands in the flap in both subunits. Residues 25–28 at the active site had the least deviation in both subunits and all structures.

Protease interactions with substrate analogs

This series of high resolution crystal structures allowed more precise description of the PR interactions with transition state mimics. Figure 4 shows the super-imposed substrate analogs in the PR_{V82A} complexes. The P2-P2′ side chains were in similar positions, while the more distal residues had greater conformational variation. PR recognizes substrates by means of a series of hydrogen bond interactions with the main chain atoms of the peptide (Fig. 5). Similar hydrogen bond interactions were observed between PR and P3-P3′ positions of the anologs, as described previously [12,25], while there was more variation at the distal ends. Two water molecules are conserved in all eight structures and mediate the interactions between the PR and the inhibitor. One conserved water molecules lies between the flap region (Ile50 and 50′) and P2 and P1′ of the inhibitor, which has been proven to be important for catalysis [30,31], and the other mediates the interactions of P2′ with Gly27′ and Asp29′.

Complex with CA-p2 analog

The CA-p2 analog bound to PR_{V82A} in two orientations with a relative occupancy of 0.65/0.35. Residues P3-P4′ of CA-p2 interacted with PR (Fig. 5A). Compared with p2-NC, the CA-p2 analog lacked an acetyl group at P4 and cannot form the same van der Waals interactions with PR. However, the CA-p2 analog with P2′ Glu had two proton-mediated hydrogen bond interactions with the Asp30 carboxylate side chain, instead of the single hydrogen bond of P2′ Gln in p2-NC (Fig. 1B), as described previously [12]. The norleucine (Nle) at P4′ in CA-p2, instead of the NH_2 in p2-NC, allowed formation of hydrogen bonds with the carbonyl oxygen of Met46′ and the side chain of Lys45′. Furthermore, P3 is Arg in CA-p2 and Thr in p2-NC. As a result, the carbonyl oxygen of P3 Arg interacted with the amide of Asp29 instead of the interaction of the amide of P3 Thr with carbonyl oxygen of Gly48 in the flap. In addition, the longer Arg side chain provided more van der Waals interactions with PR. These differences corresponded with the 25- fold stronger inhibition observed for the analog CA-p2 compared with p2-NC.

Structural comparison of the complexes with the p2-NC analog

Crystal structures were determined of complexes of the substrate analog p2-NC with PR and the two mutants PR_{V82A} and PR_{I84V}. The p2-NC showed one conformation in all three structures. The PR interactions extended over P4-P4′. The conserved hydrogen bond interactions with main chain amide and oxygen atoms extended from P3 O to P4′-N, and the P2′ Gln side chain formed hydrogen bond interactions with Asp29′ and Asp30′ in all three structures (Fig. 5B). Multiple conformations were modeled for the side chain of P1′- Nle in the mutant complexes. The main chain oxygen and hydroxyl of P3 Thr had water mediated

interactions with Gly27, Asp29 and Asp30. These conserved waters may stabilize the PR–inhibitor complex, as suggested previously [12].

There were small compensatory changes in the interactions with p2-NC in the complexes with PR_{V82A} and PR. P3′ in PR_{V82A}–p2-NC showed more interactions with water molecules than observed in the PR complex. However, it is possible that more water molecules were identified as a result of the higher resolution of the PR_{V82A}–p2-NC complex. In mutant PR_{V82A}, Ala82 had lost the van der Waals interaction with P4 Ace, and interacted more weakly with P1 (interatomic distances of more than 4.0 Å). However, the interactions at P1′ and P3′ were enhanced (Fig. 6A) mainly by movements of the side chains of P1 Nle and P3′ Arg and partially by the small (0.3 Å) shift of the CA atom of Ala82/82′. P1′-Nle showed three conformations for the side chain and had closer contacts with the CB atom of Ala82 in PR_{V82A} than observed for Val in the PR. The CE atom of P3′ Arg moved ≈1.2 Å and formed closer interactions with the CB atom of Ala82. All of these observed structural changes and closer van der Waals interactions with p2-NC were consistent with fourfold better inhibition for PR_{V82A} than for PR (Table 1). Similar small changes in the backbone atoms of residue 82 in mutant PR_{V82A} were described for complexes with nonpeptidic inhibitors [32].

Val84 in the PR_{I84V}–p2-NC complex had fewer interactions with P2 compared with those of Ile84 in the PR–p2-NC structure. Similarly to the PR_{V82A} complex, the flexibility of the P1′ Nle side chain compensated partially for the loss of van der Waals interactions caused by the shorter side chain of Val compared with Ile (Fig. 6B). These changes agreed with the sixfold weaker inhibition of p2-NC for PR_{I84V} than for PR. These structures suggest that p2-NC analog had modulated the binding affinity for mutants through small conformational changes of the side chain of P1′-Nle. Similarly, the conformational flexibility of the Met side chain in the natural substrate is expected to compensate for the drug resistant mutations, such as V82A and I84V.

Structural comparison of the complexes with the $p6^{pol}$-PR analog

The structures had two conformations of $p6^{pol}$-PR with relative occupancies of 0.6 and 0.4 and 0.8 and 0.2 for PR–$p6^{pol}$-PR and PR_{V82A}–$p6^{pol}$-PR complexes, respectively. As the $p6^{pol}$-PR analog had 11 residues and extended out of the PR-binding pocket, both N- and C-terminal residues were quite flexible, with poor electron density. On the other hand, the longer peptide provided interactions extending from P5 to P5′, as illustrated in Fig. 5C. P2 is the polar Asn, unlike the hydrophobic Val and Ile in CA-p2 and p2-NC. Hence, the side chain of P2 Asn formed hydrogen bonds with Asp29 and Asp30, which cannot occur in CA-p2 or p2-NC. The $p6^{pol}$-PR had the larger hydrophobic Phe at P3 compared with Arg, Thr or Gly in the other analogs. The P3 Phe occupied more space in the binding pocket, and fewer water-intermediated interactions were observed. The smaller amino acid, Pro, at P1′ resulted in fewer van der Waals contacts with PR than for other analogs with Phe, Nle or Leu at P1′. The two complexes showed the largest deviation from PR–p2-NC for the residues 48–52 in the flap region of both subunits. This structural change in the flaps and the differences in interactions with the substrate side chains were consistent with the poorer inhibition of PR by $p6^{pol}$-PR compared with CA-p2 and p2-NC analogs.

PR_{V82A} and PR showed almost identical hydrogen bond and van der Waals interactions with $p6^{pol}$-PR, except for interactions with the terminal P5 Val and P4′ Thr. As noted previously, the N terminus was very flexible and had two different orientations when bound to PR or PR_{V82A}. Thus, the N-terminal residues had van der Waals interactions with totally different residues in the two complexes. In the case of PR_{V82A}, the N terminus had lost the hydrogen bond at the P5 position and, instead, had a water-mediated interaction of P4 with Met46. PR–$p6^{pol}$-PR showed interactions of the C terminus of $p6^{pol}$-PR with Asp60 and Gln61 through a water molecule, while PR_{V82A}–$p6^{pol}$-PR did not have those interactions. Residue 82 interacted

with P1 and P1′ of $p6^{pol}$-PR and small shifts were observed for both Ala82 and P1 Phe in PR_{V82A}–$p6^{pol}$-PR compared with these positions in the PR complex (Fig. 6C). These structural changes resulted in good van der Waals interactions of Ala82/82′ CB atoms with P1′ Pro–P1 Phe and compensated for the loss of the methyl groups of Val82 in PR. The structural adjustment of the PR_{V82A} mutant to accommodate inhibitor binding was consistent with the similar inhibition constants observed for PR_{V82A} and PR with $p6^{pol}$-PR (36 and 22 μM, respectively).

Structural comparison of the complexes with the p1-p6 analog

The two complexes of PR–p1-p6 and PR_{V82A}–p1-p6 had two orientations of the analog with a relative occupancy of 0.6 and 0.4. Residues P5-P5′ of p1-p6 interacted with PR and PR_{V82A} (Fig. 5D). As in the p2-NC complexes, the N-terminal P4 and P3 of p1-p6 showed similar hydrogen bond and van der Waals interactions with protease; however, these differed from the interactions with $p6^{pol}$-PR. The long side chain of P4′ Arg at the C terminus formed extra water-mediated interactions with PR residues Trp6, Arg8, Asp29′, Asp30′ and Arg87′. The major difference from the other substrate analogs was the presence of the small Gly at the P3 position in p1-p6. The P3 Gly had fewer van der Waals interactions with PR, and p1-p6 had more space to move around the binding pocket. As a result, although both p1-p6 and $p6^{pol}$-PR had Asn at P2, it showed different hydrogen bonds with PR. In $p6^{pol}$-PR, the large ring of P3 Phe restricted movement in the binding site and pushed P2 Asn more towards the active site, which enabled P2 Asn to form hydrogen bonds with Asp29 and Asp30. Mean-while, with Gly at P3, the backbone of p1-p6 had moved in the binding site and provided more flexibility for P2Asn. The side chain of P2Asn in p1-p6 adopted two conformations, which differed by a rotation of ≈90°. One conformation of P2 Asn maintained weaker hydrogen bonds with Asp29 and 30, while the other conformation was surrounded by the hydrophobic side chains of Ile50′, Ile84 and P1′ Leu. Furthermore, there were more water-intermediated interactions of PR with p1-p6. The loose binding of PR and p1-p6, primarily caused by P3 Gly, was consistent with its more than 50 times weaker inhibition than that of CA-p2 and p2-NC.

Similarly to the other complexes, subtle structural changes allowed improved van der Waals interactions between PR_{V82A} and P1′ and P1 of the substrate analog compared with those of PR (Fig. 6D). The improved interactions with p1-p6 were consistent with the threefold better inhibition of PR_{V82A} than PR, and with the higher relative k_{cat} K_m for hydrolysis of the p1-p6 substrate [21].

PR interactions with substrate analogs compared to those with clinical inhibitors

Substrate analogs showed more flexibility than clinical inhibitors in binding to the mutant PRs. The high-resolution crystal structures of PR, PR_{V82A} and PR_{I84V} complexes indicated that the binding affinity for mutants was modulated by the conformational flexibility of P1 and P1′ side chains in the substrate analogs (Fig. 6). Similarly, molecular dynamic studies suggest that flexibility of substrate residues P1 and P1′ can affect catalysis [33]. It is instructive to compare the PR and mutant complexes with the clinical inhibitors. The crystal structures of PR, PR_{V82A} and PR_{I84V} with UIC-94017, an inhibitor in phase IIB clinical trials, and of PR, PR_{V82A} and PR_{L90M} with the drug indinavir, were determined at resolutions of 1.1–1.6 Å [25,34]. All these structures were superimposed on PR– UIC-94017 with root mean square deviations on alpha carbon atoms of 0.15–0.25 Å. The clinical inhibitors maximize the interactions within PR subsites S2 to S2′, while the longer substrate analogs have more extended interactions within S4 to S4′. UIC-94017 is smaller than the substrate analogs but formed similar hydrogen bonds to PR main chain atoms. Compared with indinavir and other clinical inhibitors, UIC-94017 formed more polar interactions with the main chain atoms of Asp29 and Asp30 [24]. These interactions resembled those of the P2′ Gln or Glu side chain of peptide analogs (Figs 1B and 5).

Similar rearrangements of residue 82/82′ and of P1/P1′ were observed in PR_{V82A} and in PR complexes (Fig. 6). These shifts allowed closer contacts of Ala82 and 82′ with the inhibitor, and partially compensated for the smaller side chain of Ala compared with wild-type Val. However, Ala82/82′ showed smaller shifts (0.1–0.4 Å of Cα) with substrate analogs and larger changes (0.5–0.8 Å) with clinical inhibitors. These changes were coupled with larger movements or multiple conformations of P1/P1′ side chains in substrate analogs (Fig. 6A–D) than observed for the inhibitors UIC-94017 or indinavir (Fig. 6E,F). In contrast, Val84 in PR_{I84V} was less flexible than Ala82 in PR_{V82A}, so that adaptation in the PR_{I84V}–p2-NC complex was caused by the alternate conformations of P1′ Nle (Fig. 6B). Consequently, similar K_i values for PR and PR_{V82A} were observed for both substrate analogs and UIC-94017 (0.3–1.6-fold) and increased by threefold for indinavir [31], while the K_i values increased from two- to sixfold for PR_{I84V} [25]. Similar structural changes were reported for the inactive double mutant V82A–D25N compared with the D25N mutant in complexes with peptides or ritonavir [10]. These observations suggested that the substrate analogs have more flexibility to accommodate the structural changes caused by mutation of PR. Hence, the comparison of PR complexes with substrate analogs or drugs helps to explain how the virus can develop drug resistance while retaining the ability to catalyze the hydrolysis of natural substrates.

Structure of the active site and implications for the reaction mechanism

These crystal structures of PR with reduced peptide analogs represent a transition state in the reaction. Ideally, the reaction mechanism would be analyzed using a series of crystal structures of active PR with peptide substrates and transition-state analogs representing different steps in the reaction. However, it is difficult to obtain crystal structures of active PR with peptide substrates. Two strategies have been used to analyze the structures of the transition state(s). We have analyzed structures of active PR with reduced peptide analogs that mimic the transition state of the hydrolytic reaction because they contain an amine and a tetrahedral carbon at the nonhydrolysable peptide bond. Other groups have used an alternative strategy of crystallizing an inactive enzyme with the D25N mutation in complex with peptide substrates [8–10]. There were several differences between our crystal structures of PR with peptide analogs and those of the D25N inactive enzyme with peptides. The PR sequence differed in six amino acids, in addition to the D25 N25 difference. Moreover, most of the peptides had different sequences. The two structures of D25N–p1-p6 (1KJF) and PR–p1-p6 that share similar peptide sequences were compared. Overall, the RMS differences were 0.6 Å for main chain atoms, as usually observed for PR crystal structures in different space groups. The most striking difference was in the conformation of the peptide or reduced peptide backbone atoms between P1 and P1′ (Fig. 7A). These differences arise from the presence of the planar peptide bond (CO-NH) in the peptide instead of the tetrahedral carbon in the reduced peptide (CH_2-NH). The tetrahedral carbon in the reduced peptide was much closer to the Asp25 and 25′ side chains than was the carbonyl carbon in the peptide bond (the two carbon atoms were separated by 1.1 Å). The tetrahedral carbon atom of the reduced peptide interacted with the four carboxylate oxygen atoms of Asp25 and 25′ at distances of 3.1–4.0 Å. In contrast, the peptide carbonyl oxygen of D25N–p1-p6 showed one hydrogen bond interaction and one van der Waals interaction with the carboxylate oxygens of Asp25′. Furthermore, the tetrahedral carbon in the reduced peptide was in a similar position to the tetrahedral carbon of CH-OH in the UIC-94017 inhibitor, which mimics the transition state and showed interactions of the hydroxyl group with all four Asp25/25′ carboxylate oxygen atoms (Fig. 7B). Therefore, the PR complexes with reduced peptide analogs more closely represented the tetrahedral transition state of the reaction, while the D25N–peptide structures are likely to represent the initial step of substrate binding to the PR.

Special feature in electron density map around the active site

The atomic resolution structure of PR_{V82A}–p2-NC showed unusual Fo–Fc difference density at the catalytic site that may relate to the reaction mechanism. The other crystal structures showed little or no difference density around the catalytic site. In these substrate analogs, the carbonyl group of P1 has been reduced to a methylene group to prevent hydrolysis. However, significant Fo–Fc positive difference density was observed close (≈ 1.4 Å) to the reduced carbon atom on P1 Nle (Fig. 8). Previous crystallographic studies of HIV-1 PR in complex with a pseudo-C2 symmetric inhibitor, and molecular dynamic calculations, suggested that the difluoroketone core was hydrated and that the hydration of the carbonyl group is the initial step for HIV-1 PR catalysis [35,36]. Therefore, a hydroxyl was tested in the positive density. No reduction in the difference density was observed in tests with various other atoms (H, Na or O). The positive difference density was decreased, but not eliminated, only when a hydroxyl group was added to the reduced carbon atom. The refinement used a standard Nle and a hydroxyl-Nle with relative occupancies of 0.7 and 0.3. Mass spectroscopic studies of crystals and separated peptide analog showed no significant change in molecular mass of either PR or inhibitor. Therefore, any modification of the p2-NC analog must be transient at best and occurred only in the crystal structure. Moreover, hydration of the reduced carbon is an energetically unfavorable event. Thus, it is not clear whether the hydroxyl-Nle exists. Further analysis of the data by charge density analysis or quantum calculations will be necessary to understand this difference density at the active site, and help elucidate the catalytic mechanism.

These high-resolution crystal structures of HIV PR with natural cleavage substrate analogs provide new molecular details for understanding the specificity of substrate recognition and a basic framework for the design of new inhibitors that are more effective against resistant HIV.

Experimental procedures

Expression and purification

The HIV-1 PR has been optimized for structural and kinetic studies with five mutations, as follows: Q7K, L33I, L63I to minimize the autoproteolysis of the PR, and C67A and C95A to prevent cysteine-thiol oxidation [37]. The construction and expression of HIV-1 PR, PR_{V82A} and PR_{I84V} were carried out as described previously [3,38]. The refolding and purification procedures were similar to those reported previously [37,38]. Mutations were confirmed by protein mass spectrometry.

Substrate and peptide analogs

The chromogenic substrate, L6525, was purchased from Sigma-Aldrich (St Louis, MO, USA). CA-p2- and p2-NC-reduced peptide analogs were purchased from Bachem Bio-science (King of Prussia, PA, USA). The NC-p1, p1-p6 and $p6^{pol}$-PR reduced peptides were synthesized by I. Blaha (Ferring Leciva, Prague, Czech Republic). The substrate analog inhibitors were dissolved in deionized water by vortexing for several minutes, and then centrifuged briefly to remove any insoluble material.

Crystallization and data collection

The PR or mutant was concentrated to 5 $mg \cdot mL^{-1}$ and then mixed with the inhibitor at a 20-fold molar excess. The mixture was incubated at 4 °C for 1 h and then centrifuged. Crystallization was achieved by the hanging-drop vapor-diffusion method at 297 K using 24-well VDX plates (Hampton Research, Aliso Viejo, CA, USA). Equal volumes of enzyme-inhibitor and reservoir solution were used. The screening was performed with combinations of the following solutions: 0.1 M sodium acetate buffer (pH 4.2–5.0), 0.1 M citrate phosphate

buffer (pH 5.0–6.4), 5% (v/v) dimethylsulfoxide, 0–5% (v/v) dioxane, 0.4–1.2 M sodium chloride and 15–40% (w/v) saturated ammonium sulfate.

The crystals were frozen in liquid nitrogen using glycerol as a cryoprotectant, which was added to the reservoir solution to a final concentration of 30% (v/v). X-ray diffraction data were collected at National Synchrotron Light Source, beamline X26C or Advanced Photon Source, beamline SER-CAT 22.

Data processing and refinement

The datasets collected at the National Synchrotron Light Source were processed using the HKL suite 1.96, and the other datasets collected at the Advanced Photon Source were processed by the HKL 2000 package [39]. Molecule replacement was performed using AMORE [40]. The starting model for molecular replacement was chosen from the highest resolution structure available in the space group $P2_12_12$. The structures were refined using the program SHELXL [41], and map display and refitting used the molecular graphics program O [42]. Structure solution in the $P2_1$ space group was tested when the structures showed two alternate conformations of inhibitor. Alternate conformations for PR residues, water and other solvent molecules were modeled when observed. The type of ion and other solvent molecules was identified by the shape of the 2Fo–Fc electron density map, the potential for hydrogen bonding, the coordination state and the interatomic distances, for molecules present in the crystallization conditions. Anisotropic B factors were applied. Hydrogen atoms were calculated in the last round of refinement by SHELXL (except for $p6^{pol}$-PR complexes which are low resolution). Structures were superimposed as described previously [34]. Structural figures were made using MOLSCRIPT [43] and WEBLAB viewer (Molecular Simulations Inc., San Diego, CA, USA).

Inhibition measurements

Measurements of the inhibition constant, K_i, for peptide analogs of the CA-p2, p2-NC, $p6^{pol}$-PR and p1-p6 natural PR cleavage sites, were made by spectroscopic assay with the chromogenic substrate (Lys-Ala-Arg-Val-Nle-*p*-nitro- Phe-Glu-Ala-Nle-amide, L6525; Sigma-Aldrich), which is an analog of the CA-p2 cleavage site. The assay solution contained 50 mM sodium acetate, pH 5.0, 0.1 M NaCl and 1 mM EDTA. The reaction concentrations of enzyme and the substrate were 70–120 nM and 300 μM, respectively. The PR concentrations were determined by active site titrations with indinavir, and the substrate concentration was determined by converting the absorbance of the substrate to concentration via a calibration curve. The decrease in absorbance at 310 nm of the reaction mixture was measured on a Hitachi U-2000 spectrophotometer. The inhibition curves were fit by SIGMAPLOT 8.0.2 (SPSS Inc., Chicago, IL, USA). Inhibition constants of each analog inhibitor were obtained from the 50% inhibitory concentration (IC_{50}) values estimated from a dose–response curve using the equation $K_i = (IC_{50}–0.5[E])/(1 + [S]\ K_m)$, where [E] and [S] are the PR and substrate concentrations, respectively, and K_m values were determined earlier [25].

Protein databank accession numbers

The structures have been deposited in the protein databank as 2AOD (WT–p2-NC), 2AOC (I84V–p2-NC), 2AOE (V82A– CA-p2), 2AOF (V82A–p1-p6), 2AOG (V82A–p2-NC), 2AOH (V82A–p6-PR), 2AOI (WT–p1-p6) and 2AOJ (WT–p6-PR).

Acknowledgements

This research was supported, in part, by the National Institutes of Health grants GM062920 and AIDS-FIR-CA TW01001 (I.T.W., R.W.H. and J.T.), Hungarian Science and Research Fund grants OTKA F35191 and T43482 (P.B. and J.T.), the Molecular Basis of Disease Fellowship (Y.T.), the Georgia Cancer Coalition Distinguished Cancer Scholar award (I.T.W. and R.W.H.), and the Georgia Research Alliance. We thank the staff at the SER-CAT beamline at the Advanced Photon Source, Argonne National Laboratory, and at the beamline X26C of the National Synchrotron Light Source at Brookhaven National Laboratory, for assistance during X-ray data collection. Use of the Advanced

Photon Source was supported by the U.S. Department of Energy, Basic Energy Sciences, Office of Science, under Contract No. W-31-109-Eng-38. Use of the National Synchrotron Light Source was supported by the US Department of Energy, Division of Materials Sciences and Division of Chemical Sciences, under Contract No. DE-AC02-98CH10886.

References

1. Darke PL, Nutt RF, Brady SF, Garsky VM, Ciccarone TM, Leu CT, et al. HIV-1 protease specificity of peptide cleavage is sufficient for processing of Gag and Pol polyproteins. Biochem Biophys Res Commun 1988;156:297–303. [PubMed: 3052448]
2. Oroszlan S, Luftig RB. Retroviral proteases. Curr Top Microbiol Immunol 1990;157:153–185. [PubMed: 2203608]
3. Wlodawer A, Erickson JW. Structure-based inhibitors of HIV-1 protease. Annu Rev Biochem 1993;62:543–585. [PubMed: 8352596]
4. Erickson JW, Gulnik SV, Markowitz M. Protease inhibitors: resistance, cross-resistance, fitness and the choice of initial and salvage therapies. AIDS Res Hum Retroviruses 1999;13:S189–S204.
5. Shafer RW, Winters MA, Palmer S, Merigan TC. Multiple concurrent reverse transcriptase and protease mutations and multidrug resistance of HIV-1 isolates from heavily treated patients. Ann Intern Med 1998;128:906–911. [PubMed: 9634429]
6. Shafer RW. Genotypic testing for human immunodeficiency virus type 1 drug resistance. Clin Microbiol Rev 2002;15:247–277. [PubMed: 11932232]
7. Wu TD, Schiffer CA, Gonzales MJ, Taylor J, Kantor R, Chou S, et al. Mutation patterns and structural correlates in human immunodeficiency virus type 1 protease following different protease inhibitor treatments. J Virol 2003;77:4836–4847. [PubMed: 12663790]
8. Prabu-Jeyabalan M, Nalivaika E, Schiffer CA. Substrate shape determines specificity of recognition for HIV-1 protease: analysis of crystal structures of six substrate complexes. Structure 2002;10:369–381. [PubMed: 12005435]
9. Prabu-Jeyabalan M, Nalivaika EA, King NM, Schiffer CA. Viability of a drug-resistant human immunodeficiency virus type 1 protease variant: structural insights for better antiviral therapy. J Virol 2003;77:1306–1315. [PubMed: 12502847]
10. Prabu-Jeyabalan M, Nalivaika EA, King NM, Schiffer CA. Structural basis for coevolution of a human immunodeficiency virus type 1 nucleocapsid-p1 cleavage site with a V82A drug-resistant mutation in viral protease. J Virol 2004;78:12446–12454. [PubMed: 15507631]
11. Weber IT, Wu J, Adomat J, Harrison RW, Kimmel AR, Wondrak EM, Louis JM. Crystallographic analysis of HIV-1 protease with an analog of the conserved CA–p2 substrate: Interactions with frequently occurring Glu at P2′ position of substrate. Eur J Biochem 1997;249:523–530. [PubMed: 9370363]
12. Mahalingam B, Louis JM, Hung J, Harrison RW, Weber IT. Structural implications of drug resistant mutants of HIV-1 protease: High resolution crystal structures of the mutant protease/substrate analogue complexes. Proteins Struct Funct Genet 2001;43:455–464. [PubMed: 11340661]
13. Mahalingam B, Boross P, Wang YF, Louis JM, Fischer CC, Tozser J, Harrison RW, Weber IT. Combining mutations in HIV-1 protease to understand mechanisms of resistance. Proteins Struct Funct Genet 2002;48:107–116. [PubMed: 12012342]
14. Pettit SC, Moody MD, Wehbie RS, Kaplan AH, Nantermet PV, Klein CA, Swanstrom R. The p2 domain of human immunodeficiency virus type 1 Gag regulates sequential proteolytic processing and is required to produce fully infectious virions. J Virol 1994;68:8017–8027. [PubMed: 7966591]
15. Louis JM, Nashed NT, Parris KD, Kimmel AR, Jerina DM. Kinetics and mechanism of auto-processing of human immunodeficiency virus type 1 protease from an analog of the Gag-Pol polyprotein. Proc Natl Acad Sci USA 1994;91:7970–7974. [PubMed: 8058744]
16. Croteau G, Doyon L, Thibeault D, McKercher G, Pilote L, Lamarre D. Impaired fitness of human immunodeficiency virus type 1 variants with high-level resistance to protease inhibitors. J Virol 1997;71:1089–1096. [PubMed: 8995629]
17. Robinson LH, Myers RE, Snowden BW, Tisdale M, Blair ED. HIV type 1 protease cleavage site mutations and viral fitness: implications for drug susceptibility phenotyping assays. AIDS Res Hum Retroviruses 2000;16:1149–1156. [PubMed: 10954890]

18. Zhang YM, Imamichi H, Imamichi T, Lane HC, Falloon J, Vasudevachari MB, Salzman NP. Drug resistance during indinavir therapy is caused by mutations in the protease gene and its Gag substrate cleavage sites. J Virol 1997;71:6662–6670. [PubMed: 9261388]
19. Barrie KA, Perez EE, Lamers SL, Farmerie WG, Dunn BM, Sleasman JW, Goodenow MM. Natural variation in HIV-1 protease, Gag p7 and p6, and protease cleavage sites within Gag/Pol polyproteins: amino acid substitutions in the absence of protease inhibitors in mothers and children infected by human immunodeficiency virus type 1. Virology 1996;219:407–416. [PubMed: 8638406]
20. Bally F, Martinez R, Peters S, Sudre P, Telenti A. Polymorphism of HIV type 1 gag p7/p1 and p1/p6 cleavage sites: clinical significance and implications for resistance to protease inhibitors. AIDS Res Hum Retroviruses 2000;16:1209–1213. [PubMed: 10957718]
21. Feher A, Weber IT, Bagossi P, Boross P, Mahalingam B, Louis JM, Copeland TD, Torshin IY, Harrison RW, Tozser J. Effect of sequence polymorphism and drug resistance on two HIV-1 Gag processing sites. Eur J Biochem 2002;269:4114–4120. [PubMed: 12180988]
22. Tozser J, Blaha I, Copeland TD, Wondrak EM, Oroszlan S. Comparison of the HIV-1 and HIV-2 proteinases using oligopeptide substrates representing cleavage sites in Gag and Gag-Pol polyproteins. FEBS Lett 1991;281:77–80. [PubMed: 2015912]
23. Tomasselli AG, Olsen MK, Hui JO, Staples DJ, Sawyer TK, Heinrikson RL, Tomich CS. Substrate analogue inhibition and active site titration of purified recombinant HIV-1 protease. Biochemistry 1990;29:264–269. [PubMed: 2182116]
24. Klabe RM, Bacheler LT, Ala PJ, Erickson-Viitanen S, Meek JL. Resistance to HIV protease inhibitors: a comparison of enzyme inhibition and antiviral potency. Biochemistry 1998;37:8735–8742. [PubMed: 9628735]
25. Tie Y, Boross PI, Wang YF, Gaddis L, Hussain AK, Leshchenko S, et al. High resolution crystal structures of HIV-1 protease with a potent non-peptide inhibitor (UIC-94017) active against multi-drug-resistant clinical strains. J Mol Biol 2004;338:341–352. [PubMed: 15066436]
26. Rose RB, Craik CS, Stroud RM. Domain flexibility in retroviral proteases: structural implications for drug resistant mutations. Biochemistry 1998;37:2607–2621. [PubMed: 9485411]
27. Ishima R, Freedberg DI, Wang YX, Louis JM, Torchia DA. Flap opening and dimer interface flexibility in the free and inhibitor-bound HIV protease, and their implications for function. Struct Fold Des 1999;7:1047–1055.
28. Piana S, Carloni P, Rothlisberger U. Drug resistance in HIV-1 protease: Flexibility-assisted mechanism of compensatory mutations. Protein Sci 2002;11:2393–2402. [PubMed: 12237461]
29. Perryman AL, Lin JH, McCammon JA. HIV-1 protease molecular dynamics of a wild-type and of the V82F/I84V mutant: possible contributions to drug resistance and a potential new target site for drugs. Protein Sci 2004;13:1108–1123. [PubMed: 15044738]
30. Grzesiek S, Bax A, Nicholson LK, Yamazaki T, Wingfield PT, Stahl SJ, et al. NMR evidence for the displacement of a conserved interior water molecule by a non-peptide cyclic urea based HIV protease inhibitor. J Am Chem Soc 1994;116:1581–1582.
31. Wang YX, Freedberg DI, Yamazaki T, Wingfield PT, Stahl SJ, Kaufman JD, et al. Solution NMR evidence that the HIV-1 protease catalytic aspartyl groups have different ionization states in the complex formed with the asymmetric drug KNI-272. Biochemistry 1996;35:9945–9950. [PubMed: 8756455]
32. Baldwin ET, Bhat TN, Liu B, Pattabiraman N, Erickson JW. Structural basis of drug resistance for the V82A mutant of HIV-1 proteinase. Nat Struct Biol 1995;2:244–249. [PubMed: 7773792]
33. Piana S, Carloni P, Parrinello M. Role of conformational fluctuations in the enzymatic reaction of HIV-1 protease. J Mol Biol 2002;319:567–583. [PubMed: 12051929]
34. Mahalingam B, Wang YF, Boross PI, Tozser J, Louis JM, Harrison RW, Weber IT. Crystal structures of HIV protease V82A and L90M mutants reveal changes in the indinavir-binding site. Eur J Biochem 2004;271:1516–1524. [PubMed: 15066177]
35. Slee DH, Laslo KL, Elder JH, Ollmann IR, Gustchina A, Kervinen J, Zdanov A, Wlodawer A, Wong CH. Selectivity in the inhibition of HIV and FIV protease: inhibitory and mechanistic studies of pyrrolidine-containing alpha-keto amide and hydroxyethylamine core structures. J Am Chem Soc 1995;117:11867–11878.

36. Silva AM, Cachau RE, Sham HL, Erickson JW. Inhibition and catalytic mechanism of HIV-1 aspartic protease. J Mol Biol 1996;255:321–346. [PubMed: 8551523]

37. Wondrak EM, Louis JM. Influence of flanking sequences on the dimer stability of human immunodeficiency virus type 1 protease. Biochemistry 1996;35:12957–12962. [PubMed: 8841142]

38. Louis JM, Wondrak EM, Copeland TD, Smith CA, Mora PT, Oroszlan S. Chemical synthesis and expression of the HIV-1 protease gene in *E. coli*. Biochem Biophys Res Commun 1989;159:87–94. [PubMed: 2647085]

39. Otwinowski Z, Minor W. Processing of X-ray diffraction data in oscillation mode. Methods Enzymol 1997;276:307–326.

40. Navaza J. AMoRe: An automated package for molecular replacement. Acta Crystallogr A 1994;50:157–163.

41. Sheldrick GM, Schneider TR. SHELXL: High resolution refinement. Methods Enzymol 1997;277:319–343.

42. Jones TA, Zou JY, Cowan SW, Kjeldgaard M. Improved methods for building protein models in electron density maps and the location of errors in these models. Acta Crystallogr A 1991;47:110–119. [PubMed: 2025413]

43. Kraulis PJ. MOLSCRIPT: a program to produce both detailed and schematic plots of protein structures. J Appl Crystallogr 1991;24:946–950.

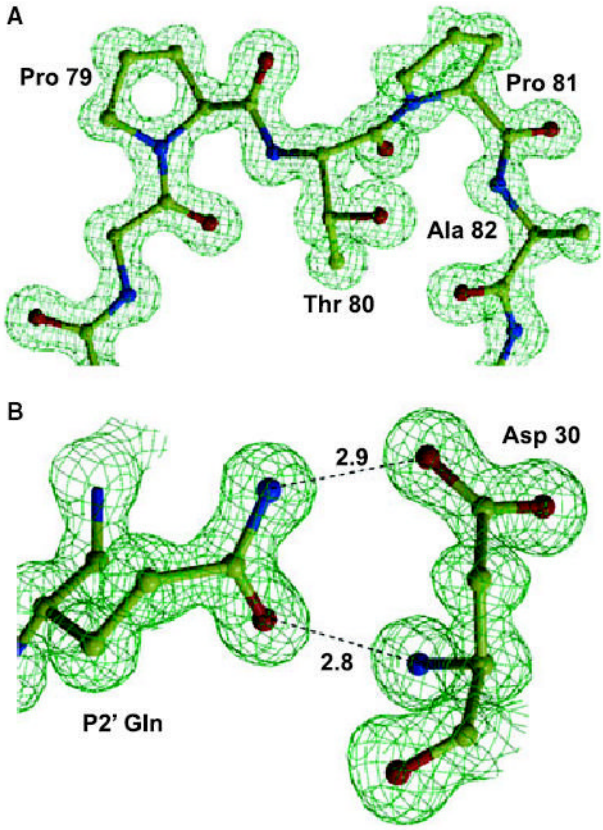

Fig. 1.

Electron density map of HIV-1 protease with the V82A mutation (PR_{V82A})–p2-NC crystal structure. The 2Fo–Fc map was contoured at a level of 2.2σ. Hydrogen bond interactions are shown with distances in Å. (A) Residues 78–82. (B) Asp30 interacting with P2′ Gln.

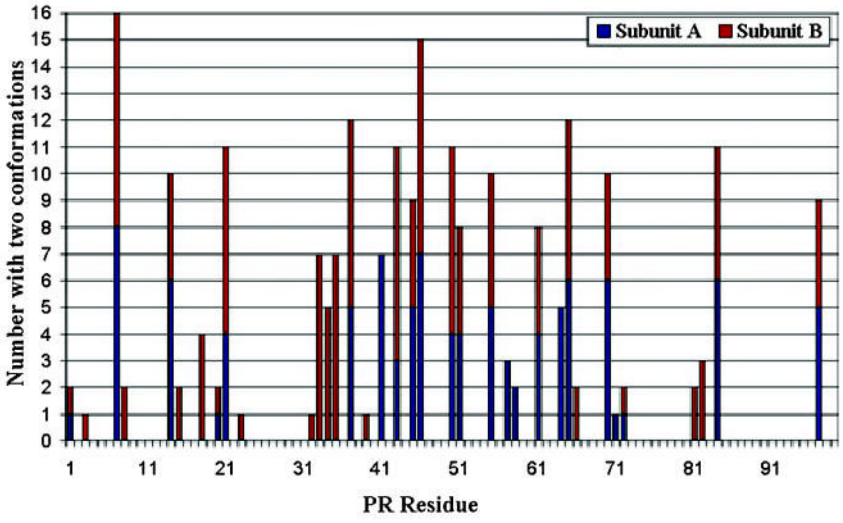

Fig. 2.

Residues with alternate conformations. The number of occurrences of alternate conformations for each residue in the A and B subunits of the eight crystal structures are shown.

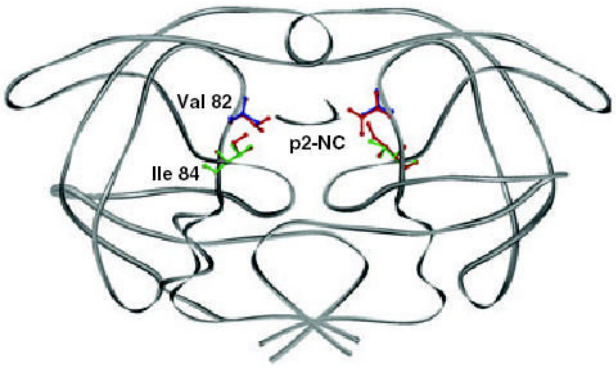

Fig. 3.

Superposition of the wild type HIV-1 protease (PR), PR with the V82A mutation (PR_{V82A}) and PR_{V82A} in complex with p2-NC. The ribbons represent the backbones of the dimers and the p2-NC analog. The sites of mutations Val82 and Ile84 are shown by red bonds for PR, blue for Ala82, and green for Val84 in both subunits.

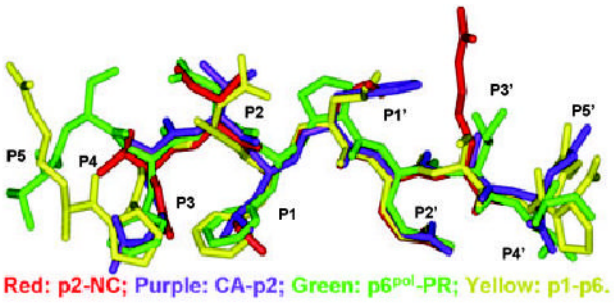

Fig. 4.

Superposition of four complexes of HIV-1 protease with the V82A mutation (PR_{V82A}) with the inhibitors CA-p2, p2-NC, $p6^{pol}$-PR and p1-p6.

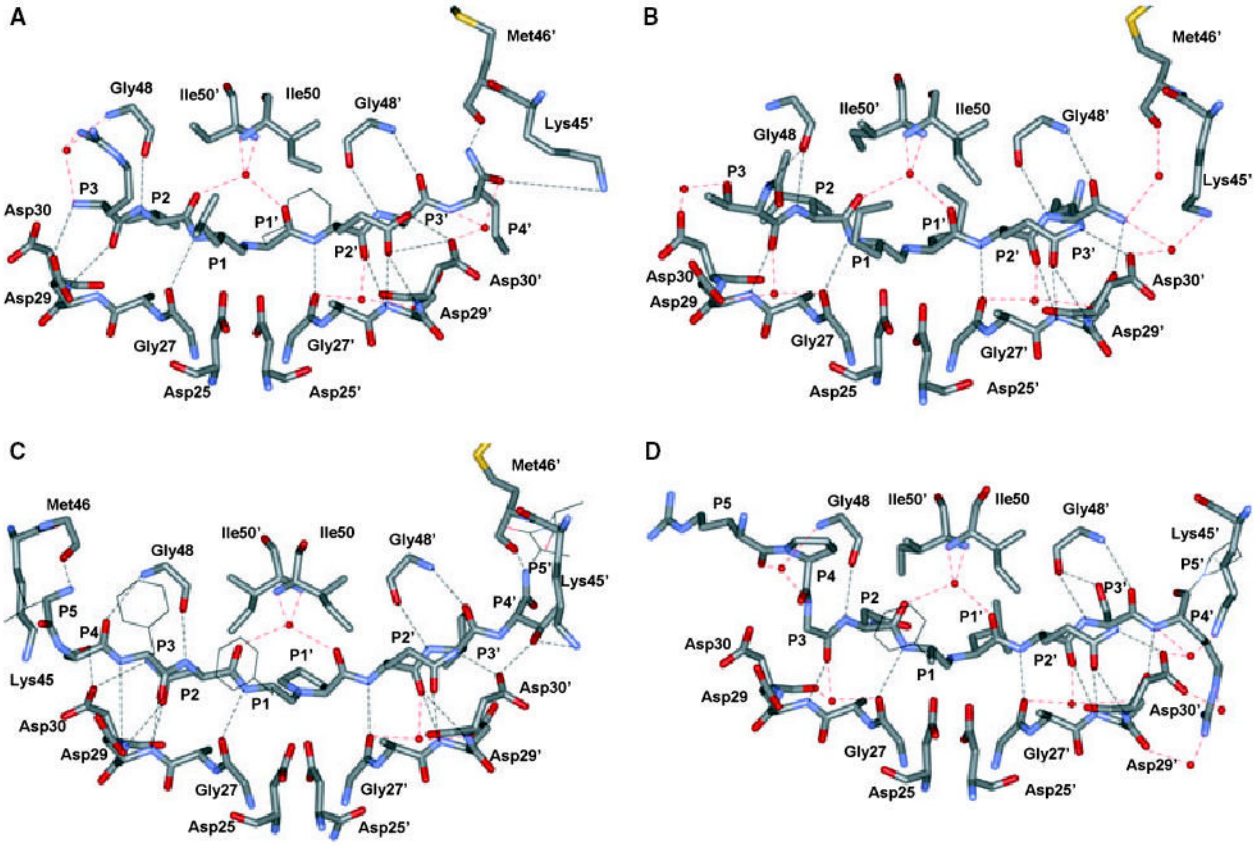

Fig. 5.

Hydrogen bond interactions between protein and inhibitor. Hydrogen bond interactions are shown for interatomic distances of 2.5– 3.3 Å. Water molecules are indicated by red spheres. Water-mediated hydrogen bonds are shown as red dashed lines, while direct interactions between the protease and inhibitor are in black. (A) Hydrogen bond interactions between HIV-1 protease with the V82A mutation (PR_{V82A}) and CA-p2. (One water-mediated interaction between P3 Arg and Pro 81′ is not shown.) (B) Hydrogen bond interactions between PR and p2-NC. (Water-mediated interactions of both termini of inhibitor with Arg8 and 8′ are not shown.) (C) Hydrogen bond interactions between PR and $p6^{pol}$-PR. (Water-mediated interactions of the C termini of $p6^{pol}$-PR with Asp60 and Gln61 are not shown.) (D) Hydrogen bond interactions between PR_{V82A} and p1-p6. (Water-mediated interactions of the C termini of p1-p6 with Trp6, Arg8 and Arg87′ are not shown.)

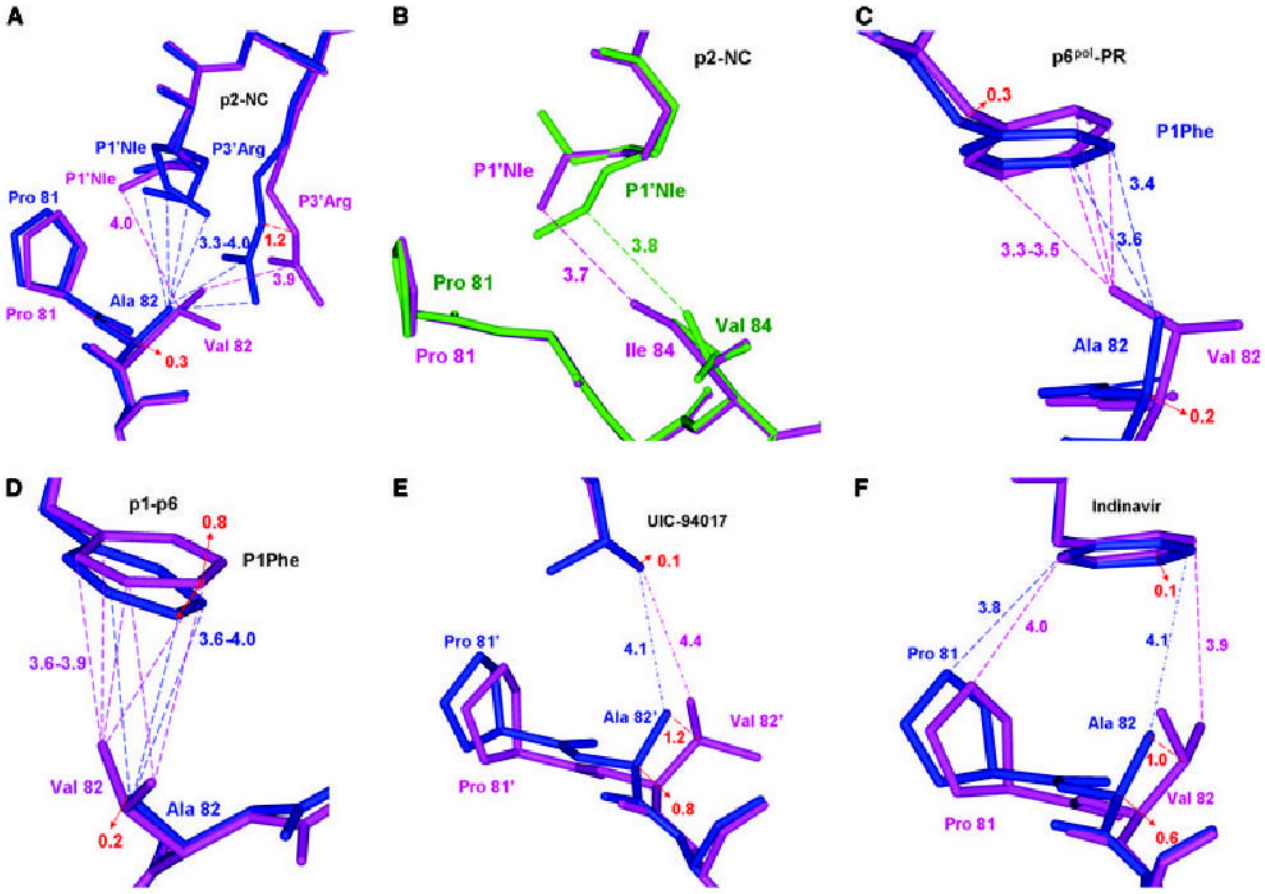

Fig. 6.

Structural variation around residues 8184 in p2-NC, $p6^{pol}$-PR, p1-p6, UIC-94017 and indinavir complexes. The protease (PR) structure is shown in purple, PR with the 184V mutation (PR_{I84V}) in green and PR with the V82A mutation (PR_{V82A}) in blue bonds. Interatomic distances (Å) are indicated as dashed lines. (A) PR_{V82A}–p2-NC superimposed on PR–p2-NC. (B) PR_{I84V}–p2-NC superimposed on PR–p2-NC. (C) PR_{V82A}–$p6^{pol}$-PR superimposed on PR–$p6^{pol}$-PR. (D) PR_{V82A}–p1-p6 superimposed on PR–p1-p6. (E) PR_{V82A}–UIC-94017 superimposed on PR–UIC-94017. (F) PR_{V82A}–indinavir superimposed on PR–indinavir.

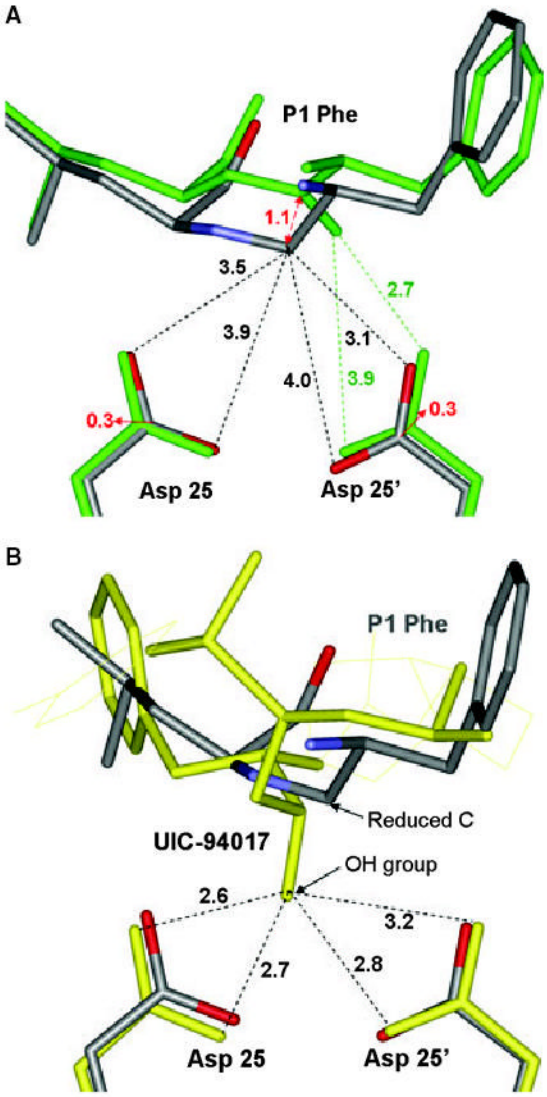

Fig. 7.

Structural variation around the active site. (A) PR–p1-p6 is shown (colored by atom type) superimposed on D25N–p1-p6 (1KJF) in green bonds. Distances within 4.0 Å are shown. (B) PR– UIC-94017 is shown as yellow bonds superimposed on PR–p1-p6 complex (colored by atom type).

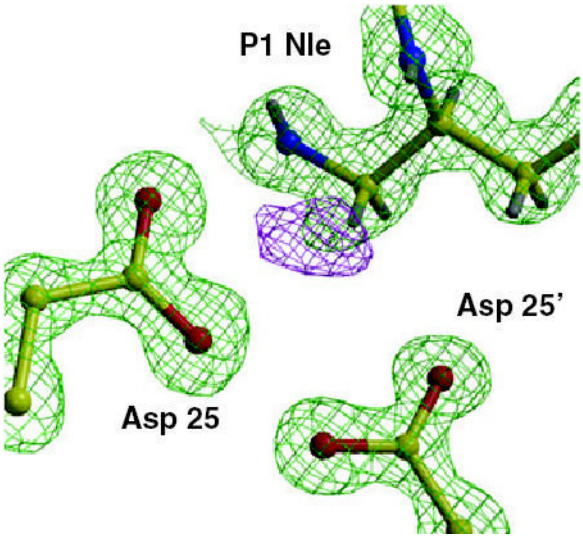

Fig. 8.

Electron density maps at the active site of the PR_{V82A}− p2-NC complex. The 2Fo-Fc map is green and was contoured at a level of 2.2, whereas the Fo-Fc map is contoured at 3.2 and colored purple for positive.

Table 1

Sequence of the substrate analog inhibitors and inhibition constants. Values are listed for K_i, in μ_M, and values in parenthesis are the K_i relative to PR. PR, wild type HIV-1 protease; PR_{V82A}, PR with the V82A mutation; PR_{I84V}, PR with the I84V mutation.

Cleavage site	Peptide sequence	PR	PR_{V82A}	PR_{I84V}
CA-p2	R-V-L-r-F-E-A-Nle	0.075 ± 0.009	0.024 ± 0.004 (0.3)	0.275 ± 0.031 (3.7)
p2-NC	Ace-T-I-Nle-r-Nle-Q-R	2.17 ± 0.28	0.53 ± 0.078 (0.24)	13.0 ± 1.5 (6.0)
$p6^{pol}$-PR	V-S-F-N-F-r-P-Q-I-T-K-K	22.1 ± 2.8	36.3 ± 5.4 (1.6)	46.6 ± 5.3 (2.1)
p1-p6	R-P-G-N-F-r-L-Q-S-R-P	96.7 ± 12.3	28.2 ± 4.2 (0.3)	> 500 (> 5)
NC-p1	E-R-Q-A-N-r-F-L-G-K-I	> 500	> 500	> 500

Table 2

Crystallographic data statistics. PR, wild type HIV-1 protease; PR_{V82A}, PR with the V82A mutation; PR_{I84V}, PR with the I84V mutation

Protease	**PR_{V82A}** [a]	**PR** [a]	**PR_{V82A}** [a]	**PR_{I84V}**	**PR**	**PR_{V82A}** [b]	***#Pr** [ab]	**PR_{V82A}**
Inhibitor	CA-p2	p2-NC	p2-NC	p2-NC	$p6^{pol}$-PR	$p6^{pol}$-PR	p1-p6	p1-p6
Space group	$P2_12_12$	$P2_12_12$	$P2_12_12$	$P2_12_12$	$P2_12_12$	$P2_12_12$	$P2_12_12$	$P2_12_12$
Unit cell dimensions (Å)								
a	57.89	58.00	58.02	57.80	59.45	58.88	58.91	58.46
b	85.96	85.78	85.89	85.59	87.00	86.27	86.07	85.85
c	46.19	46.53	46.61	46.46	46.32	46.40	46.54	46.39
Resolution range (Å)	50–1.54	50–1.40	50–1.10	50–1.30	50–1.60	50–1.42	50–1.38	50–1.32
Unique reflections	34 544	44 291	95 318	55 009	32 005	40 847	47 418	55 317
R_{merge} (%) overall (final shell)	6.5 (37.1)	10.1 (45.6)	10.2 (37.7)	7.9 (33.0)	9.1 (41.3)	9.8 (70.8)	10.4 (28.6)	8.4 (57.7)
<I/sigma> overall (final shell)	13.4 (5.8)	8.9 (2.1)	10.4 (2.1)	14.4 (3.2)	13.2 (3.7)	17.1 (2.6)	14.1 (13.8)	10.4 (2.9)
Data range for refinement (Å)	10–1.54	10–1.40	10–1.10	10–1.30	10–1.60	10–1.42	10–1.38	10–1.32
R_{work} (%)	0.12	0.15	0.13	0.12	0.15	0.18	0.16	0.13
R_{free} (%)	0.19	0.19	0.17	0.16	0.23	0.23	0.21	0.18
No. of waters (total occupancies)	194	188	206	223.5	155	199	190	297
Completeness (%)overall (final shell)	99.6 (100)	95.6 (66.6)	94.8 (68.4)	96.0 (72.4)	99.2 (93.1)	90.3 (100)	89.2 (96.2)	99.9 (100)
RMS deviation from ideality								
Bonds (Å)	0.010	0.011	0.015	0.013	0.009	0.011	0.010	0.012
Angle distance (Å)	0.029	0.029	0.033	0.030	0.029	0.031	0.030	0.034
Average B-factors ($Å^2$)								
Main chain	15.9	8.0	9.0	10.6	22.4	16.7	14.2	12.0
Side chain	21.9	12.2	13.7	15.4	27.6	21.1	18.4	17.0
Inhibitor	27.5	14.0	10.6	14.7	29.9	19.1	18.3	24.0
Solvent	31.5	23.7	24.4	25.8	37.9	30.9	27.3	26.7

[a] Diffraction data collected at Advanced Photon Source, beamline SER-CAT 22. All other data were collected at National Synchrotron Light Source, beamline X26C.

[b] Structures in which hydrogen atoms were not added.